

FEATURE ARTICLE

Structure, Topology, and Dynamics of Membrane Peptides and Proteins from Solid-State NMR Spectroscopy

Mei Hong[†]

Department of Chemistry, Iowa State University, Ames, Iowa

Received: May 13, 2007; In Final Form: July 1, 2007

The high-resolution structure of membrane proteins is notoriously difficult to determine due to the hydrophobic nature of the protein–membrane complexes. Solid-state NMR spectroscopy is a unique and powerful atomic-resolution probe of the structure and dynamics of these important biological molecules. A number of new solid-state NMR methods for determining the depth of insertion, orientation, oligomeric structure, and long-range (10–15 Å) distances of membrane proteins are summarized. Membrane protein depths can now be determined using several complementary techniques with varying site-specificity, distance precision, and mobility requirement on the protein. Membrane protein orientation can now be determined with or without macroscopic alignment, the latter providing a novel alternative for orientation determination of intrinsically curvature-inducing proteins. The novel analyses of β -sheet membrane protein orientation are described. The quaternary structure of membrane peptide assemblies can now be elucidated using a ¹⁹F spin diffusion technique that simultaneously yields the oligomeric number and intermolecular distances up to 15 Å. Finally, long-range distances up to \sim 10 Å can now be measured using ¹H spins with an accuracy of better than 1 Å. These methods are demonstrated on several β -sheet membrane peptides with antimicrobial activities and on two α -helical ion-channel proteins. Finally, we show that the nearly ubiquitous dynamics of membrane proteins can be readily examined using 2D correlation experiments. An intimate appreciation of molecular motion in these systems not only leads to important insights into the specific function of these membrane proteins but also may be exploited for other purposes such as orientation determination.

1. Introduction

Membrane-bound proteins are ubiquitous in cells, and carry out a myriad of important functions. They convert light energy to chemical energy, transport ions and metabolites into and out of the cell, and transduce chemical signals across the membrane.¹ Membrane peptides and proteins can also interact with lipid membranes in a destructive way, for example, when the innate immune system of a host organism generates peptides that kill invading pathogens by disrupting their cell membranes.² To understand the mechanism of action of membrane proteins, it is crucial to determine their three-dimensional structure on the atomic length scale, elucidate their orientation and depth of insertion in the membrane, and understand functionally relevant conformational dynamics.

Solid-state NMR spectroscopy has been traditionally used to study the chemical and three-dimensional structures of organic and inorganic solids.^{3,4} However, the intrinsic atomic-level structural information, the nonperturbing nature, and the large range of dynamic time scales (10^{-10} –1 s) of solid-state NMR spectroscopy also make it a natural technique for determining protein structure in the solid state. The insoluble and noncrystalline membrane proteins,^{5–8} along with fibrous and aggregating

proteins,⁹ are ideal systems to be investigated using solid-state NMR. The large molecular weight of the lipid–protein assemblies prevents them from undergoing fast isotropic tumbling in solution, thus prohibiting high-resolution solution NMR spectroscopy to be used for structure determination. The hydrophobic nature of membrane proteins and protein–lipid mixtures also makes them difficult to crystallize; thus, X-ray crystallography is not generally applicable to membrane proteins. Solid-state NMR spectroscopy does not impose these sample restrictions and allows membrane protein structure to be determined in their native environment of lipid bilayers.

2. Depth of Insertion of Membrane Proteins

One of the first questions about the topology of membrane proteins is their depth of insertion. Integral and peripheral membrane proteins have vastly different insertion depths. For many membrane-lytic peptides, knowing the depths of insertion often gives valuable clues to their mechanism of action. For example, some antimicrobial peptides reside on the membrane surface and at high concentration cause of membrane disruption by micellization.¹⁰ Other antimicrobial peptides form transmembrane pores^{11–13} that insert all the way to the hydrophobic core of the lipid bilayer.

We have developed several NMR methods to determine the depth of insertion of membrane proteins either site-specifically or globally. The first method is paramagnetic relaxation

[†] Present address: Department of Chemistry, Gilman 0108, Iowa State University, Ames, IA 50011. Phone: 515-294-3521. E-mail: mhong@iastate.edu.

Mei Hong, John D. Corbett Professor of Chemistry at Iowa State University, received her B.A. in 1992 from Mount Holyoke College and her Ph.D. in chemistry in 1996 from the University of California at Berkeley. She then spent one year as a NIH postdoctoral fellow at the Massachusetts Institute of Technology and two years at the University of Massachusetts Amherst as a research professor. Since joining the faculty of Iowa State University in 1999, she has focused her research on the development and application of solid-state NMR techniques to the determination of the structure and dynamics of membrane proteins, with a special emphasis on membrane protein topology. She also investigates the conformation of structural proteins such as elastin and collagen.

enhancement (PRE), where paramagnetic ions such as Mn^{2+} bind to the phosphate groups on the membrane surface and broaden the nuclear spin signals by enhancing their T_2 relaxation in a distance-dependent manner.¹⁴ The paramagnetic contribution to transverse relaxation, T_2^P , depends on the average electron-nucleus distance, r ,^{15,16} according to

$$\frac{1}{T_2^P} = W \frac{1}{15} \left(\frac{\mu_0}{4\pi} \right)^2 \gamma_c^2 \mu_{\text{eff}}^2 \beta^2 \frac{1}{r^6} \left(4\tau_s + \frac{3\tau_s}{1 + \omega_c^2 \tau_c^2} + \frac{13\tau_s}{1 + \omega_e^2 \tau_c^2} \right) \quad (1)$$

where the correlation time, τ_s , is the inverse sum of the electronic spin–lattice relaxation time, T_{1e} , the rotational correlation time of the molecule, τ_r , and the residence time of the Mn^{2+} near the nuclear spin, τ_m :

$$\frac{1}{\tau_s} = \frac{1}{T_{1e}} + \frac{1}{\tau_r} + \frac{1}{\tau_m} \quad (2)$$

In eq 1, W is the local concentration of the Mn^{2+} ions, γ_c is the gyromagnetic ratio of the detected ^{13}C spin, μ_0 is the vacuum permeability, μ_{eff} is the effective magnetic moment of Mn^{2+} , and β is the Bohr magneton. ω_c and ω_e represent the ^{13}C and electron-spin Larmor frequencies, respectively.

The correlation time, τ_s , is difficult to measure experimentally, so the absolute electron-nucleus distances cannot be easily obtained from T_2^P quantitatively. However, the distance can be measured semiquantitatively by comparing the PRE effect of the peptide with that of the lipids, since the depths of lipid functional groups are well-known from joint X-ray and neutron diffraction analysis of biological membranes.^{17,18} Figure 1a shows the ^{13}C spectra of Mn^{2+} -free and Mn^{2+} -bound DLPC bilayers containing a β -sheet antimicrobial peptide, protegrin-1 (PG-1).¹⁴ The Mn^{2+} PRE effect is manifested as intensity reduction or line broadening of the ^{13}C signals. The lipid carbons closest to the membrane surface, which are the headgroup and glycerol backbone carbons, experience the largest intensity reduction, whereas the acyl chain carbons retain more intensities. Plotted as a function of the position from the membrane surface, the relative intensity of the lipid carbons increases monotonically from the membrane surface to the membrane center (Figure 1b).¹⁴ This depth-dependent PRE curve depends on the Mn^{2+} concentration: at low Mn^{2+} concentrations, the steepest part of the curve lies near the membrane surface, whereas, at high Mn^{2+} concentrations, the largest intensity change occurs near the bilayer center. Thus, one can adjust the Mn^{2+} concentration to tune the distance sensitivity of the technique.

Using this Mn^{2+} PRE effect, we measured the depths of insertion of several residues in PG-1 bound to DLPC bilayers. Four residues were labeled with ^{13}C . It was found that residues F12 and G2 experience the largest intensity reduction due to PRE, and thus lie near the membrane surfaces. In contrast,

residues L5 and V16 are more shielded from the paramagnetic ions and are inserted into the carbonyl and C3 carbons of the acyl chains, respectively. Since F12 and G2 lie on opposite sides of L5 and V16 in the amino acid sequence, the relative depth profile of the four residues indicates that F12 and G2 must face the two opposite surfaces of the lipid bilayer, making PG-1 a fully transmembrane peptide.¹⁴

The extraction of quantitative distances from the PRE effect assumes that the membrane peptide and the lipids have similar mobilities, so that the τ_s values for the two molecules are similar. Thus, the experiment is most applicable to relatively small and mobile membrane peptides. For large immobilized membrane proteins, we have developed a lipid-to-protein ^1H spin diffusion experiment to determine the depth of insertion.¹⁹ In the pulse sequence, the ^1H magnetization of mobile lipids and water is first selected with a T_2 filter and then allowed to transfer to the rigid protein. The transfer is then detected via the protein ^{13}C signals. Only when the protein is inserted into the hydrophobic core of the membrane will there be significant lipid chain–protein ^1H – ^{13}C cross-peaks. The intensity buildup of these cross-peaks gives a semiquantitative measure ($\pm 2 \text{ \AA}$) of the minimum distance separation between the protein and the hydrophobic core of the bilayer. This 2D ^1H – ^{13}C correlation experiment is conducted in the liquid-crystalline (LC) phase of the membrane to make spin diffusion within the lipid matrix the rate-limiting step. Once the ^1H magnetization diffuses to any residue in the protein, it is rapidly equilibrated in the entire protein due to its rigidity. Therefore, the depth information is not residue-specific but instead is about the global topology of the protein. However, this information, while still crude, may not be available otherwise for large membrane proteins.

We applied this 2D ^1H spin diffusion technique to PG-1 bound to various lipid membranes, including POPC,²⁰ POPE/POPG, and POPC/cholesterol bilayers.²¹ The POPC bilayer serves as a model membrane, whereas the anionic POPE/POPG (75:25) membrane mimics the bacterial inner membrane. The neutral POPC/cholesterol (55:45) membrane mimics the composition of eukaryotic membranes such as red blood cell membranes. The lipid chain–peptide cross-peaks rose rapidly with time in POPC and POPE/POPG membranes but much more slowly in POPC/cholesterol bilayers (Figure 2). Thus, the depth of insertion of PG-1 depends on the membrane composition: the peptide is well inserted into POPC and POPE/POPG bilayers, in close contact with the lipid acyl chains, while it is excluded from the surface of POPC/cholesterol membranes, $\sim 20 \text{ \AA}$ from the chain methyl protons. Since the plateau of the CH_2 or CH_3 buildup curves is referenced to the equilibrium intensity in the 1D ^1H direct-excitation spectrum, the 100% intensity at spin diffusion equilibrium seen in Figure 2b rules out depth heterogeneities: it is not possible for the peptide to be transmembrane in some domains of the POPE/POPG membrane but surface-bound in others.

Comparative studies of an analogous β -hairpin antimicrobial peptide, tachyplestin-I (TP-I), give a very different insertion state. Even in anionic membranes to which TP-I is attracted, the lipid–peptide cross-peaks are weak and do not increase quickly with the mixing time. These suggest that TP-I inserts only into the glycerol backbone region, at the interface between the hydrophobic chains and polar water.²² Independent orientation determination and ^{13}C – ^{31}P distance measurements confirmed that TP-I is roughly parallel to the membrane plane,²³ $\sim 7 \text{ \AA}$ from the lipid–water interface. Thus, the membrane-bound topologies of these two β -sheet peptides differ significantly. While both PG-1 and TP-I have similar numbers of cationic residues and a

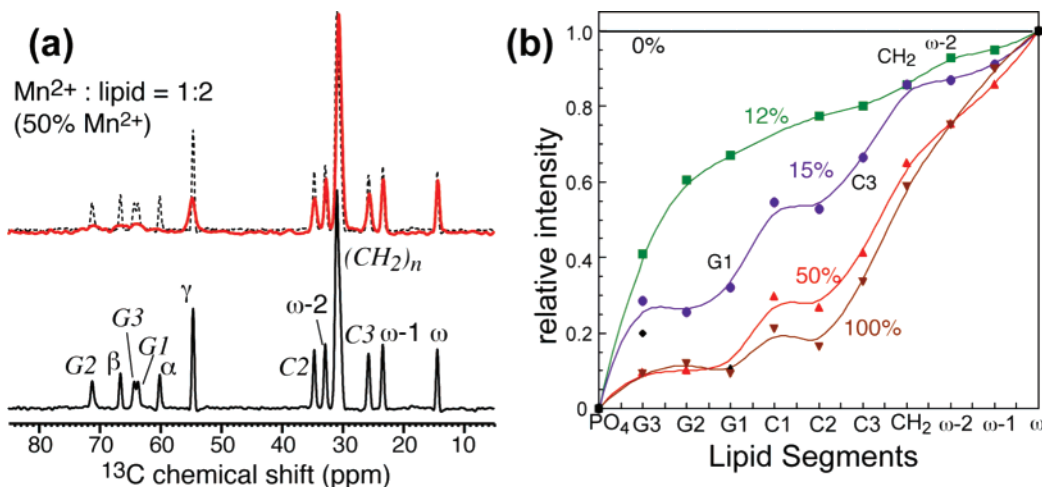


Figure 1. Mn^{2+} paramagnetic relaxation enhancement for determining the depth of insertion of membrane peptides. (a) ^{13}C MAS spectra of DLPC bilayers without (black) and with (red) Mn^{2+} . The Mn^{2+} /lipid molar ratio is 1:2 (50% Mn^{2+}). (b) ^{13}C signal intensity as a function of the depths of lipid functional groups for several Mn^{2+} concentrations. The molar concentration of Mn^{2+} is specified relative to the lipids.

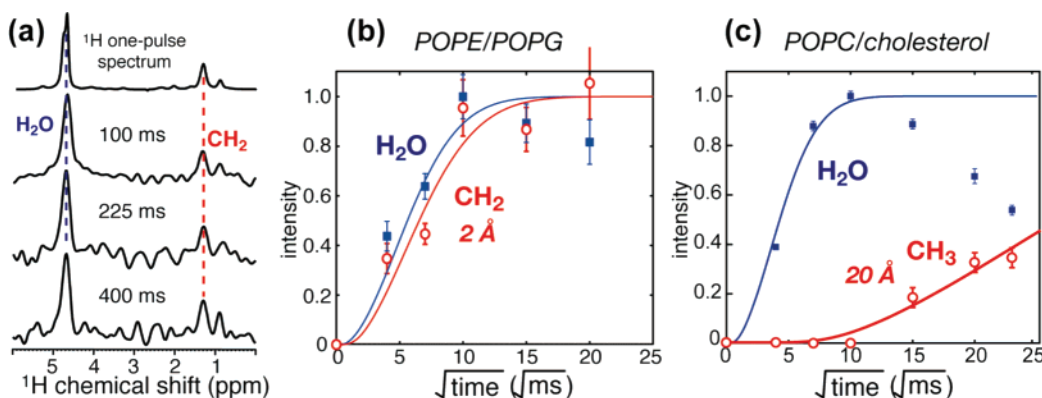


Figure 2. 2D ^1H spin diffusion data of PG-1 in different lipid membranes.²¹ (a) ^1H cross sections of PG-1 bound to POPE/POPG membranes. At 100 ms, the CH_2 signal has reached its full intensity by comparison with the direct-excitation spectrum at the top. (b) Spin diffusion buildup curves for H_2O and CH_2 cross-peaks for the POPE/POPG membrane. Both buildup curves rise rapidly, corresponding to 2 Å distances from the peptide. (c) CH_3 and H_2O buildup curves for the POPC/cholesterol sample. The CH_3 intensity buildup is much slower and corresponds to a 20 Å distance to the peptide.

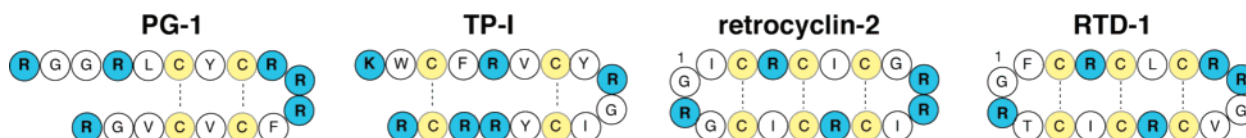


Figure 3. Amino acid sequences of several β -sheet antimicrobial peptides. Note the presence of a large hydrophobic patch in the middle of the PG-1 strands. This lengthwise amphiphilicity is reduced in the other three peptides, which may explain their different depths of insertion and antimicrobial activities.

similar disulfide-linked sequence, PG-1 is more amphipathic: it has a large hydrophobic patch in the middle of the two β -strands that is well separated from the cationic ends of the molecule. In comparison, the hydrophobic residues in TP-I are interspersed by Arg residues (Figure 3). Thus, the cause of the different insertion states of the two peptides is likely the inability of the less amphipathic TP-I to integrate into the hydrophobic part of the lipid bilayer.

3. Orientation of Membrane Peptides in Lipid Bilayers

NMR frequencies not only depend on the electronic environment of the nuclear spins but also on the orientation of the spin interaction tensors in the magnetic field, \mathbf{B}_0 . Unlike isotropic liquids where the fast isotropic tumbling of the molecules average the orientation-dependent frequencies to only the isotropic component, in immobile or partially mobile solids, this

orientation dependence is retained. The anisotropic frequency, ω , is

$$\omega = \frac{1}{2} \delta (3 \cos^2 \theta_{\text{PL}} - 1 - \eta \sin^2 \theta_{\text{PL}} \cos 2\phi_{\text{PL}}) + \omega_{\text{iso}} \quad (3)$$

where the anisotropy parameter, δ , and the asymmetry parameter, η , describe the magnitude and symmetry of the spin interaction tensor, respectively. For the chemical shift interaction, (δ, η) indicate the electronic shielding of the nuclear spins, while, for the dipole–dipole coupling, δ is the coupling constant and $\eta = 0$ by definition. The polar coordinates $(\theta_{\text{PL}}, \phi_{\text{PL}})$ describe the orientation of \mathbf{B}_0 relative to the spin interaction tensor. The subscript PL denotes the transformation from the principal axis system (PAS) of the tensor to the laboratory frame of \mathbf{B}_0 .

The membrane protein orientation of interest is the orientation relative to the bilayer normal (also called the director, D). Thus,

the angles of interest are (θ_{PD}, ϕ_{PD}) . Since lipid vesicles normally exhibit all possible orientations relative to \mathbf{B}_0 , the angles (θ_{PL}, ϕ_{PL}) are randomly distributed. Thus, the frequency spectrum of a static proteoliposome sample is a powder pattern, even though the protein has a unique set of (θ_{PD}, ϕ_{PD}) in the lipid bilayer. The NMR spectra of membrane proteins in unoriented liposomes therefore generally do not contain orientation information.

3.1. Orientation Determination Using Uniaxially Aligned Lipid Bilayers. To extract (θ_{PD}, ϕ_{PD}) of the membrane protein, the most common strategy is to align lipid bilayers macroscopically so that all protein molecules have the same (θ_{PL}, ϕ_{PL}) angles. By definition, the alignment axis is the bilayer normal axis. When this is parallel to the direction of \mathbf{B}_0 , then $\theta_{PD} = \theta_{PL}$ and $\phi_{PD} = \phi_{PL}$. Thus, the measured frequency, $\omega_{0^\circ \text{ aligned}}$, of a sample whose alignment axis is parallel to \mathbf{B}_0 is

$$\omega_{0^\circ \text{ aligned}} = \frac{1}{2} \delta(3 \cos^2 \theta_{PD} - 1 - \eta \sin^2 \theta_{PD} \cos 2\phi_{PD}) + \omega_{\text{iso}} \quad (4)$$

Since the orientation angles are now unique, a single frequency rather than a powder pattern is obtained. To align the membranes with their normal parallel to the direction of \mathbf{B}_0 , one can use either mechanical means via glass plates⁸ or magnetic alignment via flipped bicelles.^{24–28}

When the alignment axis deviates from \mathbf{B}_0 by an angle of β , then the protein in the membrane will generally have a distribution of orientations in the magnetic field and thus a distribution of frequencies. However, if the protein undergoes fast uniaxial rotational diffusion around the bilayer normal, then it can be shown that a single frequency is measured at²³

$$\bar{\omega}_{\beta \text{ tilted}} = \frac{1}{2} (3 \cos^2 \beta - 1) \cdot \frac{1}{2} \delta(3 \cos^2 \theta_{PD} - 1 - \eta \sin^2 \theta_{PD} \cos 2\phi_{PD}) + \omega_{\text{iso}} \quad (5)$$

Again, because (θ_{PD}, ϕ_{PD}) no longer samples the entire orientational space, sharp peaks rather than powder patterns are obtained whose frequencies reflect the protein orientation. Tilted alignment is encountered when glass plates are rotated in the magnetic field or when unflipped bicelles are used, whose normal is perpendicular ($\beta = 90^\circ$) to \mathbf{B}_0 due to their intrinsic anisotropic magnetic susceptibility. The condition of fast uniaxial rotation is satisfied when the bicelles undergo fast uniaxial rotations in solution and/or when the protein has intrinsic mobility in the lipid membrane.^{29,30}

Using macroscopically aligned membranes, we have measured the orientation of several β -sheet antimicrobial peptides. Different nuclear spin interactions were utilized for this purpose. For PG-1, we measured the ^{13}C chemical shift anisotropy (CSA) and the ^{15}N CSA. The latter is traditionally used for determining the orientation of α -helical membrane peptides, because of the favorable property that the main ^{15}N chemical shift tensor axis is approximately parallel to the helical axis.⁸ However, in β -sheet peptides, the ^{15}N chemical shift tensor is perpendicular to the β -strand axis, making it less sensitive to the β -sheet orientation. In comparison, the ^{13}C chemical shift tensor is exquisitely sensitive to the β -strand orientation: the most downfield principal axis (~ 245 ppm) of the tensor is along the β -strand axis, while the most upfield principal axis (~ 100 ppm) is pointed along the normal of the β -sheet plane. What this means is that a transmembrane β -sheet peptide in a 0° -aligned sample would have a CO chemical shift frequency of ~ 245 ppm, whereas an in-plane β -sheet peptide would resonate

near 100 ppm. We measured both the ^{13}C and ^{15}N chemical shifts of site-specifically labeled PG-1 bound to DLPC bilayers (Figure 4a,b). The anisotropic chemical shifts constrained the β -strand axis to be 55° from the bilayer normal (Figure 4c).³¹

We also used the 2D N–H dipolar and ^{15}N chemical shift correlation technique, commonly applied to α -helical membrane proteins,⁸ to determine the orientation of a cyclic β -hairpin antimicrobial peptide, retrocyclin-2.³² Because the orientation of the ^{15}N chemical shift tensor deviates slightly from the N–H bond, which is the direction of the dipolar tensor, correlation of the dipolar coupling and chemical shift frequencies in 2D yields characteristic patterns that depend on the tilt angle, τ , of the main molecular axis. For α -helical proteins, these patterns are elliptical and are called PISA wheels.^{33,34} The size and position of the PISA wheels depend on the tilt angle of the helical axis from the bilayer normal, while the frequency of each residue on the PISA wheel reflects the rotation angle, ρ , of that residue around the helical axis. A change in rotation angle does not affect the shape and position of the PISA wheel in the spectra but the positions of the resonances on the wheel. Thus, resonance assignment is necessary for determining the helical rotation angle. On the other hand, the 2D spectral patterns of β -sheet proteins have more complex shapes that depend not only on the tilt angle of the β -strands but also on the rotation angle of the β -sheet plane. Thus, even without resonance assignment, simulation of the 2D spectral pattern can yield both the tilt and rotation angles. In other words, the 2D spectra of β -sheet peptides do not have rotation-angle degeneracy: different (τ, ρ) values give distinct patterns, in contrast to α -helical peptides.

The 2D N–H dipolar/ ^{15}N chemical shift correlation spectrum of uniaxially aligned retrocyclin-2 in DLPC bilayers is shown in Figure 4d. Comparison with simulated spectra indicates that the two β -strands of the peptide are almost exactly parallel to the bilayer normal (Figure 4e).³² Since a monomeric β -hairpin molecule has unsatisfied hydrogen bonds between backbone N–H and C=O groups, whose polar nature makes them unfavorable for interacting with the hydrophobic part of the membrane, the transmembrane orientation suggests that retrocyclin-2 may be oligomerized so that intermolecular hydrogen bonds can form between the polar groups to stabilize the peptide–lipid interaction.

3.2. Orientation Determination Using Unoriented Liposomes. While the uniaxial alignment strategy for orientation determination is conceptually simple, it is practically challenging due to the difficulty of preparing well-aligned membranes. This problem can be circumvented by realizing that powder samples can in fact be used for orientation determination.²³ Equation 5 implies that, under the condition that the protein undergoes fast uniaxial rotational diffusion around the bilayer normal, orientation information can be obtained from the singularities of the motionally averaged powder spectra, even though the bilayer normal is generally not parallel to the magnetic field. The equivalence between a powder sample of uniaxially mobile molecules and an oriented sample can be illustrated as follows.²³ The frequency of an immobile 0° -aligned sample depends on the polar coordinates of \mathbf{B}_0 in the principal axis system of the interaction tensor according to eq 4 (Figure 5a). The uniqueness of the orientation angles (θ_{PD}, ϕ_{PD}) gives rise to a single frequency. Uniaxial rotation around the bilayer normal in this 0° -aligned sample does not change the frequency, since the rotation is also around \mathbf{B}_0 and does not affect the peptide orientation in the magnetic field (Figure 5b). For a mobile but unoriented sample, the motional axis is generally not along \mathbf{B}_0 ,

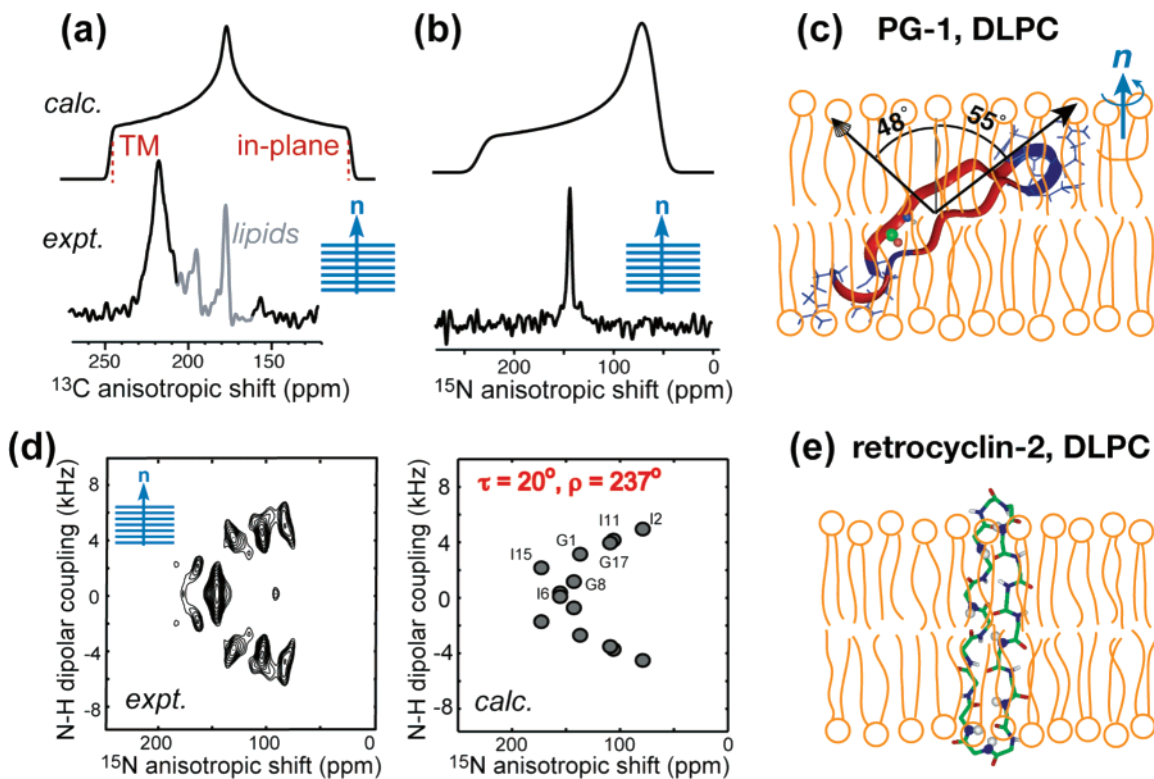


Figure 4. Orientation and depth of insertion of two β -hairpin antimicrobial peptides. (a–c) PG-1. (d, e) Retrocyclin-2. Glass-plate-aligned samples were used to obtain the spectra. (a) Calculated unoriented and experimental oriented ^{13}C spectrum of V16 in PG-1. (b) Calculated unoriented and measured oriented ^{15}N spectrum of V16 in PG-1. (c) PG-1 orientation in DLPC bilayers. (d) Experimental (left) and simulated (right) 2D N–H dipolar/ ^{15}N chemical shift correlation spectrum of multiply ^{15}N -labeled retrocyclin-2. (e) Retrocyclin-2 orientation in DLPC bilayers.

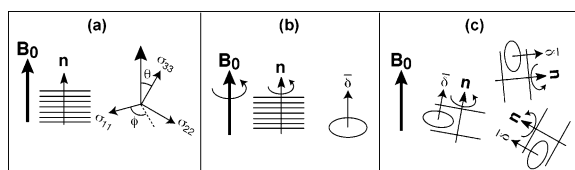


Figure 5. Schematics of the relation between oriented-sample and powder-sample spectra. (a) A 0° -oriented and immobilized system. (b) A 0° -oriented and axially mobile system. (c) An unoriented and axially mobile system.

and the NMR frequency depends on the motionally averaged anisotropy parameter, $\bar{\delta}$ (Figure 5c). This $\bar{\delta}$ is the difference from the isotropic frequency when \mathbf{B}_0 points along the unique axis of the averaged tensor, which is the motional axis. Since the motional axis, the bilayer normal, is also the alignment axis, it follows that

$$\begin{aligned}\bar{\delta} &\equiv \omega_{0^\circ \text{ aligned}} - \omega_{\text{iso}} \\ &= \frac{1}{2} \delta (3 \cos^2 \theta_{\text{PD}} - 1 - \eta \sin^2 \theta_{\text{PD}} \cos 2\phi_{\text{PD}})\end{aligned}\quad (6)$$

The motionally averaged anisotropy, $\bar{\delta}$, together with the averaged asymmetry parameter, $\bar{\eta}$, of 0, completely determine the powder line shape. The $\bar{\delta}_{\parallel}$ edge of this powder pattern, which results from bilayer normals that are parallel to \mathbf{B}_0 , appears at

$$\bar{\delta}_{\parallel} = \bar{\delta} + \omega_{\text{iso}} = \omega_{0^\circ \text{ aligned}} \quad (7)$$

Thus, the $\bar{\delta}_{\parallel}$ edge of the motionally averaged powder spectrum is identical to the frequency of the 0° -aligned sample, and the orientation of membrane proteins undergoing fast uniaxial rotation can be extracted from the powder spectra of unoriented samples.

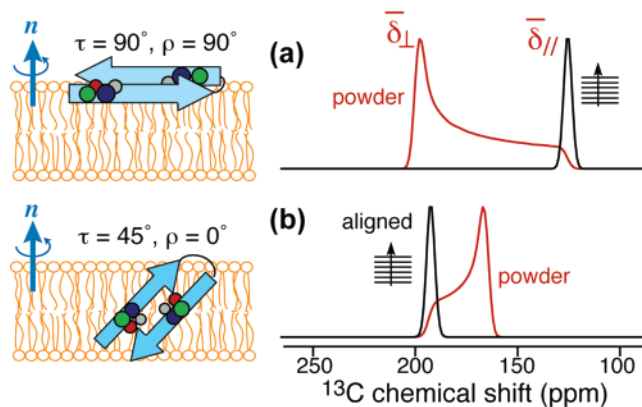


Figure 6. Calculated static ^{13}C O chemical shift spectra for two representative orientations of a β -sheet peptide, demonstrating the identity between the $\bar{\delta}_{\parallel}$ edge of the powder spectrum (red) and the frequency of the 0° -aligned sample (black).

Figure 6 shows the calculated motionally averaged ^{13}C O chemical shift spectra for several orientations of a β -sheet peptide. As an example, a β -sheet peptide lying in the plane of the lipid bilayer, which is described by $\tau = \rho = 90^\circ$, gives rise to a ^{13}C O chemical shift powder spectrum where the $\bar{\delta}_{\parallel}$ edge is close to the σ_{33} principal value. This is also the frequency of the 0° -aligned spectrum. When the peptide orientation is tilted, both the powder line shape and the 0° -aligned frequency change dramatically, but the $\bar{\delta}_{\parallel}$ edge of the powder spectrum is always identical to the 0° -aligned peak. Experiments on PG-1 under oriented and unoriented conditions confirmed this frequency equivalence between mobile unoriented samples and oriented samples.²³ Since the $\bar{\delta}_{\parallel}$ edge of the motionally narrowed powder pattern has low intensity, a practical alternative is to use the high-intensity $\bar{\delta}_{\perp}$ edge to determine the orientation, since the

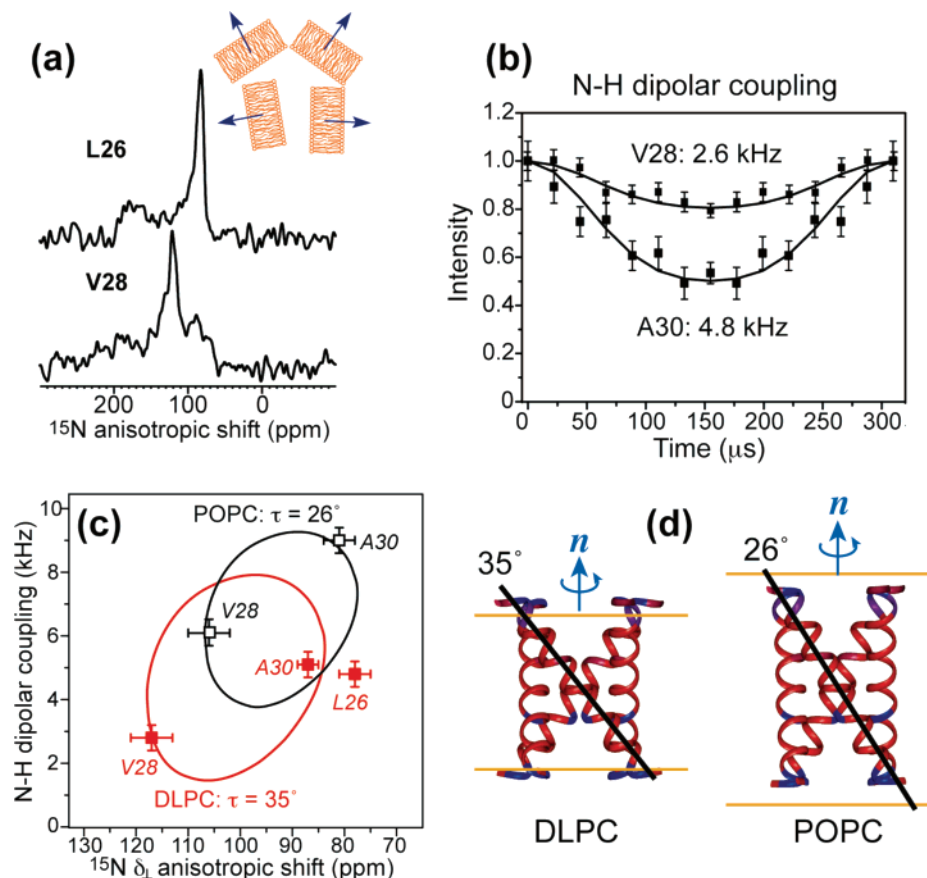


Figure 7. Determination of M2TMP orientation using unoriented proteoliposomes. (a) Static ^{15}N chemical shift powder spectra of L26 and V28 in DLPC-bound peptide. (b) N–H dipolar couplings of V28 and A30 in DLPC-bound M2TMP, extracted from the indirect dimension of 2D DIPSHIFT spectra³⁸ measured under MAS. (c) Construction of the PISA wheels of M2TMP in DLPC bilayers (red) and in POPC bilayers (black) by correlating the ^{15}N δ_{\perp} chemical shift with the N–H dipolar coupling ($\bar{\delta}_{\parallel}$). (d) Different tilt angles of M2TMP in DLPC and POPC bilayers to minimize the hydrophobic mismatch.³⁷

$\bar{\delta}_{\perp}$ frequency is related to $\bar{\delta}_{\parallel}$ by a factor of $-1/2$ from the isotropic frequency.

How commonly do membrane proteins undergo the fast uniaxial rotational diffusion required for this powder-sample approach? This is in fact quite common, since lipid bilayers form a two-dimensional solvent in which the protein undergoes both translational and rotational Brownian motions.³⁵ While the viscosity of the liquid-crystalline lipid bilayer is higher than water, the theoretically predicted rotational diffusion rates are still much higher than many NMR spin interactions for small membrane proteins. The rotational axis is usually the bilayer normal due to the symmetry of the two-dimensional membrane. Experimentally, rigid-body uniaxial rotation has been reported for a number of membrane peptides whose molecular weights are up to ~ 20 amino acid residues, and ^2H quadrupolar coupling and ^{15}N chemical shift interaction have been used for detecting the motion.³⁶ Recently, we investigated the dynamics of a tetrameric helical bundle, the M2 transmembrane peptide (M2TMP) of influenza A virus, with an effective molecular weight of ~ 11 kDa, and found that the helical bundle undergoes uniaxial rotation around the bilayer normal sufficiently fast to average the ^2H spectra of methyl-deuterated Ala.³⁷ Since ^2H quadrupolar coupling is the largest spin interaction in proteins, the smaller interactions such as ^{15}N chemical shift anisotropy and N–H dipolar coupling are also averaged by the same motion. Indeed, motionally averaged chemical shift anisotropies and dipolar couplings are obtained for multiple backbone labels such as C α and ^{15}N , which support the whole-body rotation of the M2TMP helical bundle.³⁷ We expect that if only ^{15}N and ^{13}C spin interactions are used, then membrane proteins larger

than 11 kDa should also be sufficiently mobile to yield motionally averaged spectra for orientation determination.

Taking advantage of the uniaxial mobility of M2TMP, we measured the peptide's ^{15}N chemical shift anisotropies and N–H dipolar couplings at multiple residues to extract the orientation information. The experiments were carried out on unoriented membrane samples under either static or magic-angle spinning (MAS) conditions. From the ^{15}N CSA spectra, we readily read off the $\bar{\delta}_{\perp}$ frequency from the spectral maximum (Figure 7a). From the DIPSHIFT time curves, we obtain the motionally averaged dipolar couplings, $\bar{\delta}_{\parallel}$ (Figure 7b). These two frequencies were then correlated in a 2D fashion to give a pseudo-PISA wheel spectrum (Figure 7c). Simulations of these pseudo-PISA wheels gave a helix tilt angle of 35° for DLPC-bound M2TMP but 26° for POPC-bound M2TMP. Thus, M2TMP reduces its tilt angle in the thicker lipid membrane to better match the hydrophobic thickness of the bilayer (Figure 7d).³⁷ Simplification of the sample preparation procedure made it possible to determine the effect of environmental factors (here membrane thickness) on protein orientation.

Using this powder-sample approach, we also determined the orientation of TP-I, a β -hairpin antimicrobial peptide found in horseshoe crabs.³⁹ The ^{13}C O and ^{15}N powder spectra (Figure 8) confirm motional narrowing, and indicate that the two β -strands are tilted by $\sim 20^\circ$ from the plane of the DLPC membrane.²³ This in-plane orientation is very different from the topologies of PG-1 and retrocyclin-2, and is consistent with Fourier transform infrared (FT-IR) spectra of TP-I.⁴⁰

Given the similarity of the amino acid sequences for PG-1, TP-I, and retrocyclin-2 (Figure 3), their distinct depths of

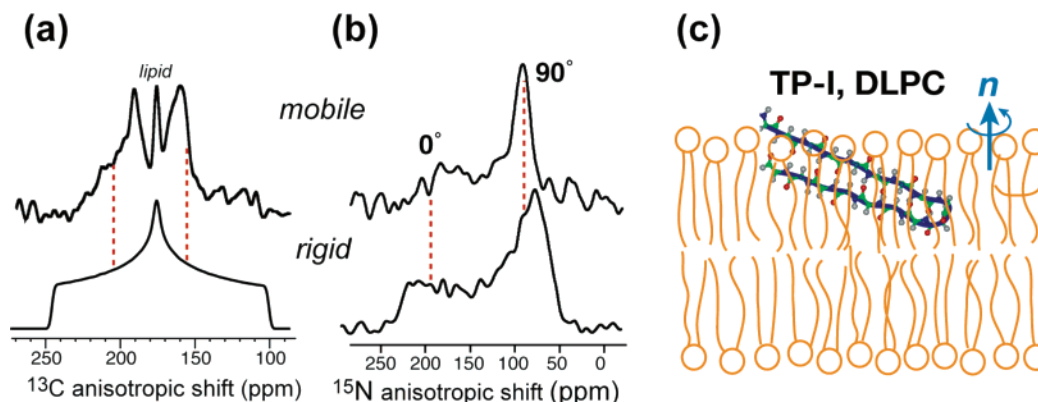


Figure 8. TP-I orientation in DLPC bilayers from powder-sample NMR. (a) Experimental motionally averaged static spectrum (top) and calculated rigid-limit spectrum (bottom) of ^{13}C -labeled V6 in TP-I. (b) Static ^{15}N chemical shift spectra of F4 in the liquid-crystalline phase (top) and the gel phase (bottom). The narrower width of the top spectrum indicates motional averaging of the chemical shift interaction. (c) TP-I orientation in DLPC bilayers based on the two chemical shift constraints.

insertion and orientations are intriguing. Again, we believe this difference originates from the different distributions of the charged and hydrophobic residues in these peptides. TP-I contains three Arg residues in the middle of the β -strands, while PG-1 and retrocyclin-2 have only one or two Arg residues in the middle of the β -strands. Thus, TP-I is the least amphipathic peptide among the three, which should reduce its tendency to insert into the hydrophobic part of the lipid bilayer. The NMR data indicate that the mechanisms of action of β -hairpin peptides are diverse: even small changes in the primary sequence can lead to entirely different mechanisms of membrane disruption.

Lipid membranes containing lytic peptides such as TP-I are, by their nature, difficult to align. The powder-sample approach thus opens up a general avenue for determining the orientation of these peptides. The use of unoriented samples also permits facile adjustment of membrane composition, pH, ion concentration, and membrane thickness to determine how environmental factors influence protein orientation. Finally, the powder-sample approach allows magic-angle spinning techniques, the most widely used solid-state NMR technology, to be employed for orientation determination.

4. Oligomeric Structure of Membrane Proteins in Lipid Bilayers

The oligomerization of membrane proteins is important for function. Channel proteins utilize oligomerization to form functional pores to conduct ions and water. Membrane-lytic peptides are thought to oligomerize to inflict maximal damage to the lipid membrane. To understand the structural basis of membrane protein function, it is thus important to determine the protein's quaternary structure in addition to the secondary and tertiary structures. However, high-resolution information on protein quaternary structure, which falls on the nanometer length scale, is difficult to obtain unless single crystals of these membrane proteins can be prepared. It is therefore desirable to extend the length scale of solid-state NMR spectroscopy from the angstrom range to the nanometer range to address this type of structural question.

Until recently, solid-state NMR spectroscopy could only measure precise distances up to ~ 5 Å. With the use of high-gyromagnetic-ratio nuclear spins such as ^{19}F and ^{31}P , the measurable distance range has increased to 8–10 Å. However, it remained difficult to determine the oligomeric number of membrane proteins and to measure distances above 10 Å. We developed a ^{19}F spin diffusion NMR technique based on the CODEX technique⁴¹ to determine both the oligomeric number

and long-range (> 10 Å) intermolecular distances in membrane protein assemblies. The experiment uses two trains of rotation-synchronized 180° pulses to recouple the anisotropic ^{19}F chemical shift interaction to create a stimulated spin echo. The intensity of the echo decreases when the chemical shift frequency changes before and after a mixing time, during which spin diffusion or molecular reorientation occurs. When molecular motions are appropriately frozen, the frequency can only change when the magnetization of one spin transfers to an adjacent spin with a different orientation. This spin diffusion process is driven by distance-dependent dipole couplings: the closer the spins, the faster the spin diffusion. At equilibrium, the fraction of magnetization residing on the initial spin without the orientational change is $1/n$, where n is the number of spins in the cluster. Thus, the equilibrium echo intensity becomes $1/n$.⁴²

Since the rate of spin diffusion depends on the distance, the CODEX decay curve must contain internuclear distance information. For spin diffusion among n spins, the mixing-time-dependent decay of magnetization, $\bar{M}(t)$, is described by the equation⁴³

$$\frac{d\bar{M}(t)}{dt} = -\hat{\mathbf{K}}\bar{M}(t) \quad (8)$$

where $\hat{\mathbf{K}}$ is an n -dimensional exchange matrix containing rate constants, k_{ij} . Detailed balance of equilibrium magnetization requires that the sum of each column of the $\hat{\mathbf{K}}$ matrix be zero and that the rate constants satisfy $k_{ij} = k_{ji}$ for equal populations of equilibrium magnetization.⁴⁴ For example, the exchange matrix of a three-spin system, ABC, is

$$\hat{\mathbf{K}} = \begin{pmatrix} k_{AB} + k_{AC} & -k_{BA} & -k_{CA} \\ -k_{AB} & k_{BA} + k_{BC} & -k_{CB} \\ -k_{AC} & -k_{BC} & k_{CA} + k_{CB} \end{pmatrix} \quad (9)$$

The formal solution to eq 8 for a given initial magnetization, $\bar{M}(0)$, is

$$\bar{M}(t) = e^{-\hat{\mathbf{K}}t}\bar{M}(0) \quad (10)$$

The exponential operator can be treated by diagonalization of the $\hat{\mathbf{K}}$ matrix or calculated directly using matrix-based software. Expressed in terms of the diagonalized exchange matrix, $\hat{\mathbf{D}}$,

$$\bar{M}(t) = \hat{\mathbf{R}}e^{-\hat{\mathbf{D}}t}\hat{\mathbf{R}}^{-1}\bar{M}(0) \quad (11)$$

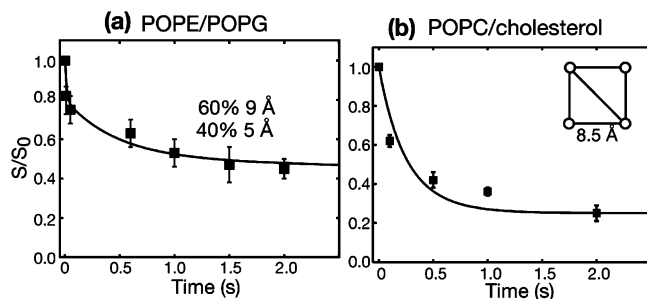


Figure 9. ^{19}F CODEX data of PG-1 in POPE/POPG (a) and POPC/cholesterol membranes (b). Each peptide is singly labeled with a ^{19}F at Phg₁₂; thus, spin diffusion is purely intermolecular. The anionic membrane gave dimers (a), whereas the neutral POPC/cholesterol membrane gave tetramers (b).

where $\hat{\mathbf{R}}$ is the eigenvector matrix of $\hat{\mathbf{K}}$. For an $n \times n$ exchange matrix with zero-sum columns, it can be shown that one eigenvalue is always zero with the associated eigenvector of $(1/\sqrt{n}, 1/\sqrt{n}, \dots, 1/\sqrt{n})$, whereas all other eigenvalues of $\hat{\mathbf{K}}$ are positive. As a result, at long mixing times, $M(t)$ approaches $(1/n, 1/n, \dots, 1/n)$, which corresponds to complete equilibration of the initial magnetization.

The rate constant, k_{ij} , is given by first-order perturbation theory as^{45,46}

$$k_{ij} = 0.5\pi\omega_{ij}^2 F_{ij}(0) \quad (12)$$

where ω_{ij} is the homonuclear dipolar coupling

$$\omega_{ij} = \frac{\mu_0}{4\pi} \gamma^2 \hbar \frac{1}{r_{ij}^3} \frac{(1 - 3 \cos^2 \theta_{ij})}{2} \quad (13)$$

This dipolar coupling depends on the internuclear distance, r_{ij} , and the angle, θ_{ij} , between the internuclear vector and \mathbf{B}_0 . $F_{ij}(0)$ is the overlap integral describing the probability that single-quantum transitions occur at the same frequency for spins i and j :

$$F_{ij}(0) = \int_{-\infty}^{+\infty} f_i(\omega - \omega_i) f_j(\omega - \omega_j) d\omega \quad (14)$$

where $f_i(\omega - \omega_i)$ is the normalized single-quantum line shape of spin i in the absence of proton decoupling and ω_i is the center of the line shape.

The parameter $F_{ij}(0)$ is difficult to calculate on the basis of first principles but can be evaluated from model compounds with known structure and similar fluorinated functional groups as those used in proteins. We measured the ^{19}F CODEX curves of crystalline 5- ^{19}F -Trp and 4- ^{19}F -2'-nitroacetanilide. Fitting the experimental decay with the known intermolecular distances resulted in a consensus $F(0)$ value of 37 μs for a spinning speed of 8 kHz. On the basis of the model compound data, we estimate that the ^{19}F CODEX technique can detect internuclear distances up to 15 Å.

Using the ^{19}F CODEX method, we determined the oligomeric structure of PG-1 in the bacteria-mimetic anionic POPE/POPG membrane and the eukaryote-mimetic neutral POPC/cholesterol membrane. In the anionic membrane, spin clusters of 2 were found for ^{19}F labels positioned at the C-terminal strand as well as the N-terminal strand, indicating that the peptide forms ...NCCNCCN... oligomers with like-strand interfaces (Figure 9a).²¹ The oligomers are inserted into the hydrophobic core of the membrane on the basis of the ^1H spin diffusion data. Thus, PG-1 forms transmembrane β -barrels in the anionic lipid

membrane. In contrast, in neutral POPC/cholesterol bilayers, PG-1 forms larger spin clusters of at least 4 for each ^{19}F label, suggesting the assembly of β -sheets (Figure 9b). ^1H spin diffusion spectra further indicate that this assembly lies on the surface of the POPC/cholesterol membrane, far from the lipid acyl chains.²¹ Thus, the oligomeric assemblies of PG-1 (Figure 10) are tuned by the membrane composition, and the different modes of assembly provide a natural molecular explanation for the selective antimicrobial activity of this peptide.

The striking difference in the packing and location of PG-1 in the two lipid membranes indicates that the 100-fold reduced membrane-lytic activity of PG-1 against eukaryotic cells is due to cholesterol's ability to prevent PG-1 insertion. Cholesterol may achieve this by rigidifying the membrane and by inducing negative curvature strain to counter peptide insertion. The β -barrel structure of PG-1 in the anionic membrane revises the well-known toroidal pore model of antimicrobial peptides, in that the peptides are not monomeric and do not act as fillers to the lipids at the pore.¹¹ Instead, it is the lipids that appear to act as fillers to a rigid and well-defined peptide barrel that defines the pore.

5. Determination of Long Distances

In addition to the ^{19}F spin diffusion technique, we also explored the high-frequency ^1H spin to measure long-range distances of ~ 10 Å with high precision (± 1 Å).⁴⁷ Most solid-state NMR distance techniques have so far utilized low-frequency nuclei such as ^{13}C and ^{15}N because of the ease of obtaining high-resolution spectra under high-power ^1H decoupling and MAS. The limiting factor in using the naturally abundant and high-frequency ^1H spins for longer-range distance measurements is the strong and multispin ^1H - ^1H homonuclear dipolar coupling in rigid solids, which cannot be spun away under conventional MAS speeds.

To obtain site-specific ^1H -X distances, we tag the ^1H spin of interest with a heteronuclear label such as ^{15}N or ^{13}C . For example, we can measure the distance from an amide proton H^{N} to a ^{13}C spin. In the experiment, the dipolar evolution of all ^1H spins by the ^{13}C label is monitored under ^1H - ^1H homonuclear decoupling. The dipolar modulation of the tagged H^{N} is then selected by a short polarization transfer step to the directly bonded ^{15}N . In this way, we obtain the distance between a single H^{N} and a single ^{13}C label. The basic pulse sequence for ^1H -X dipolar recoupling is REDOR.

With this new ^1H -X REDOR method, we showed that hydrogen bond lengths between an amide H^{N} and a ^{13}CO could be measured accurately, which provides a direct method for investigating hydrogen bonding in proteins. We also demonstrated the measurement of distances between side chain protons and backbone ^{15}N or between side chain carbons and backbone amide proton in order to determine torsion angles. For example, a distance of 7.7 Å between an ^{15}N -labeled H^{N} of Leu and the 4- ^{19}F of Phe in the tripeptide formyl-MLF⁴⁸ constrained the Phe χ_1 and ϕ torsion angles (Figure 11a).⁴⁹

We applied this ^1H -X REDOR experiment to the determination of the oligomeric structure of PG-1 in POPC membranes. To define the packing of two β -hairpins, a 1:1 mixture of a ^{13}CO -labeled PG-1 and ^{15}N -labeled PG-1 was prepared and the H^{N} -CO dipolar coupling across the oligomeric interface was measured. The REDOR dephasing curve (Figure 11b) gave distances of 2.6 and 6.7 Å, the unequal values characteristic of parallel β -strands.⁵⁰

Other long-range heteronuclear distances can be measured using the high-frequency spin ^{19}F . For example, in PG-1, we

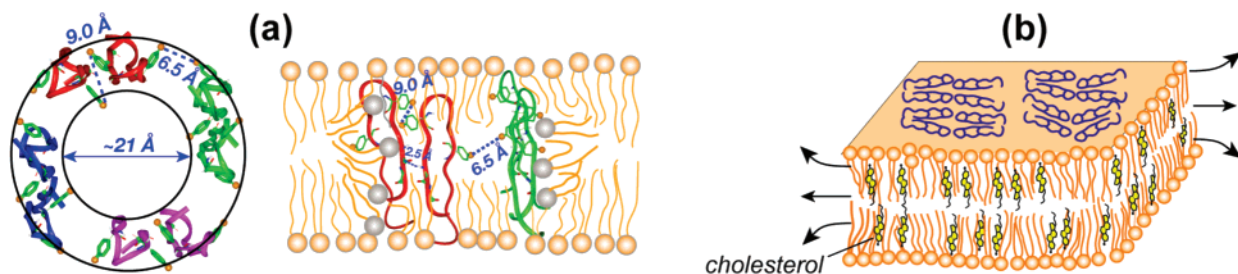


Figure 10. Oligomeric structure and insertion of PG-1 in anionic membrane versus neutral cholesterol-containing membranes. (a) Top and side views of the PG-1 β -barrel in POPE/POPG membranes. The 21 Å diameter of the barrel is estimated from leakage assay data. For clarity, the side view shows only two PG-1 dimers as part of the β -barrel. (b) PG-1 β -sheets on the POPC/cholesterol membrane surface.²¹

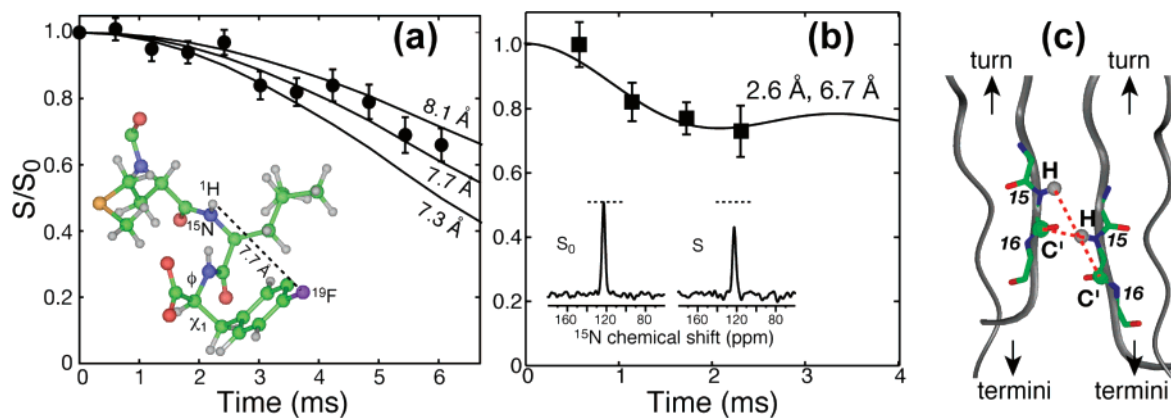


Figure 11. ^1H -X distance determination. (a) ^{15}N -detected ^1H - ^{19}F distance in formyl-MLF between Leu H^{N} and Phe 4- ^{19}F . The 7.7 Å distance constrains the Phe ϕ and χ_1 torsion angles. (b) ^{15}N -detected H^{N} -CO REDOR data of a 1:1 mixture of Cys₁₅ ^{13}C -labeled PG-1 and Cys₁₅ ^{15}N -labeled PG-1 in the POPC membrane. The distances are 2.6 and 6.7 Å (1:1). (c) The measured distances across the PG-1 dimer interface.

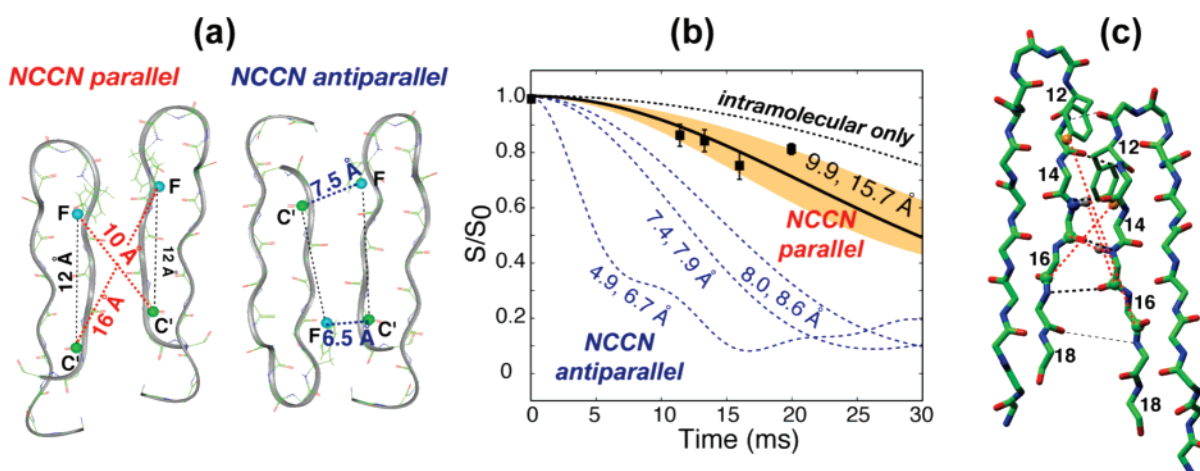


Figure 12. ^{13}C - ^{19}F distances in PG-1 bound to POPC bilayers. (a) Parallel and antiparallel NCCN packing motifs give very different distances between V16 ^{13}C and F12 ^{19}F . (b) ^{13}C - ^{19}F REDOR data. The slow decay rules out the antiparallel model. (c) Dimer model of PG-1 in POPC bilayers from experimental distance constraints (PDB: 1ZY6).

measured a ^{13}C - ^{19}F distance between V16 and F12.⁵⁰ The result indicates unequivocally that the peptides are packed in a parallel fashion, since long C-F distances of ~ 10 and ~ 16 Å were found (Figure 12).

6. Site-Specific Quantitative Depth of Insertion by X- ^{31}P REDOR

The 2D ^1H spin diffusion experiment described above gives the overall topology of the protein—whether the protein is transmembrane or peripheral—but not residue-specific depths. The paramagnetic relaxation enhancement technique yields site-specific distances from the membrane surface, but is only semiquantitative because it relies on calibration with lipids. Both of these methods also require the membrane protein to have

appropriate mobility. Thus, it is desirable to develop a general method to measure the depths of insertion residue-specifically and accurately. ^{13}C - ^{31}P or ^{15}N - ^{31}P distances between the protein and the lipids are ideal parameters for this purpose and can be measured readily using the well-established REDOR technique.⁵¹

A practical aspect to consider in conducting REDOR experiments between proteins and lipids is that the abundant motions of lipids must be frozen: any motional averaging of the coupling prevents the extraction of accurate distances. Typically, the sample needs to be ~ 50 °C below the gel-to-liquid-crystalline phase transition temperature (T_m) of the membrane to freeze the lipid headgroups. A common lipid of biological membranes is POPC, whose T_m value is -2 °C. Thus, ^{13}C - ^{31}P REDOR

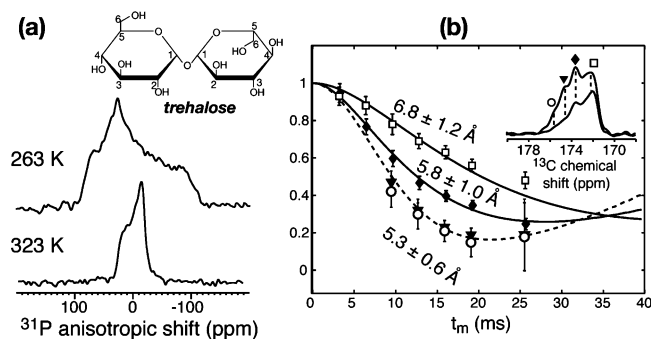


Figure 13. Trehalose cryoprotection of the POPC membrane gives rise to immobilized lipid headgroups. (a) ^{31}P static line shape of trehalose-POPC at -10 and 50 °C. The -10 °C spectrum has reached the rigid limit, whereas the 50 °C line shape corresponds to the $L\alpha$ phase. (b) ^{13}C - ^{31}P REDOR data for *sn*-1 and *sn*-2 ^{13}C O of the two POPC molecules in the unit cell. The four distances match molecular dynamics simulation results of gel-phase POPC bilayers.⁵³

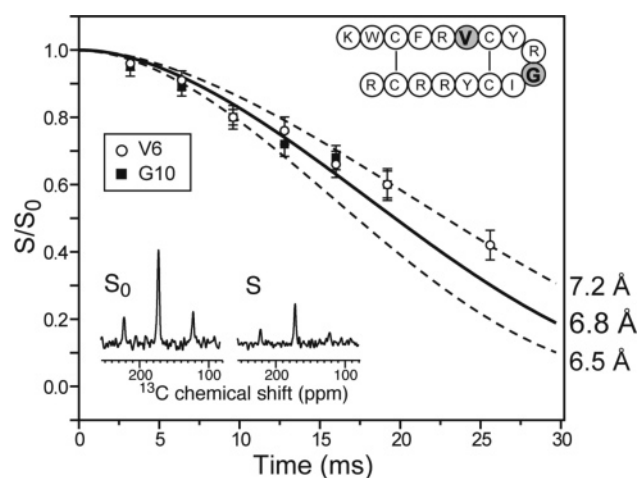


Figure 14. ^{13}C - ^{31}P REDOR data of TP-I in trehalose-protected DMPC/DMPG membrane. The V6 ^{13}C O and G10 ^{13}C O distances to ^{31}P are both 6.8 Å.

experiments would require temperatures of -50 °C or lower for long periods of time. One can ameliorate this inconvenience by using the cryoprotectant trehalose, which preserves the bilayer structure in the absence of water. Depending on the amount of trehalose mixed with the lipids, the T_m value of the dry membrane is enhanced to varying extents compared to the hydrated membrane. For example, with 20% (by mass) trehalose, the T_m value of dry POPC membrane increases to 50 °C (Figure 13a) and fully rigid ^{31}P CSA is obtained at a mild temperature of -10 °C, compared to -40 °C for the hydrated membrane. At -10 °C, ^{13}C - ^{31}P distance measurements on ^{13}C O-labeled

POPC gave intramolecular distances that are consistent with the conformation of gel-phase POPC lipids (Figure 13b), indicating that trehalose helps in immobilizing the headgroup and glycerol backbone of lipid molecules without changing the conformation.⁵²

Using ^{13}C - ^{31}P REDOR on trehalose-protected lipid membranes, we measured the depths of V6 ^{13}C O and G10 ^{13}C O in TP-I bound to DMPC/DMPG membranes and found identical distances of 6.8 Å (Figure 14). Combined with the orientation data in Figure 8, this indicates that TP-I lies at the interface between water and the hydrophobic chains, parallel to the plane of the bilayer.²² The ^{13}C - ^{31}P experiment was carried out at a mild temperature of -20 °C using trehalose-protected DMPC/DMPG membranes.

7. Membrane Protein Dynamics

An indispensable aspect of membrane protein structural biology is protein dynamics. Both local and global motions reflect protein function. For example, antimicrobial peptides can use whole-body rotation as a mechanism to disrupt the membrane integrity. Proteins that undergo conformational changes to insert into the lipid membrane or ion channels that open and close in response to external stimuli exhibit conformational plasticity necessary for these functions.

The most robust solid-state NMR strategy for obtaining site-resolved dynamics information employs 2D chemical shift and dipolar correlation spectroscopy to measure heteronuclear X-H or homonuclear H-H dipolar couplings. The heteronuclear couplings can be measured with the DIPSHIFT³⁸ or 2D LG-CP⁵⁴ pulse sequences, whereas the H-H dipolar couplings can be measured using the WISE experiment.⁵⁵ These experiments probe the couplings of fixed-distance nearest-neighbor spin pairs, which have fixed strengths in the absence of motion, so that any reduction from the rigid-limit value is indicative of motional averaging. The rigid-limit value for the C-H dipolar coupling is ~ 22 kHz and for the H-H dipolar coupling is ~ 55 kHz for protonated functional groups. Motions faster than these spin interactions scale the couplings by a factor called the order parameter, which depends on the motional amplitude.

We have measured C-H and N-H dipolar couplings using the DIPSHIFT and LG-CP experiments in several membrane proteins and peptides to determine the amplitudes of motion. In the colicin Ia channel domain, a 10-helix soluble protein that spontaneously inserts into lipid membranes through large conformational changes, we found the protein to exhibit much smaller order parameters in the membrane-bound state than in the water-soluble state (Figure 15), indicating that membrane binding enhances colicin mobility.⁵⁶ This suggests that the

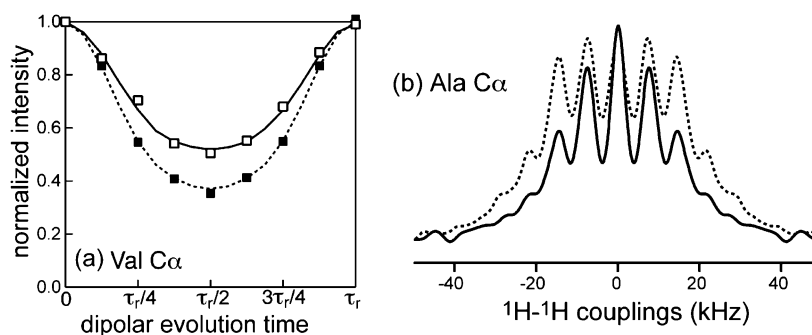


Figure 15. Dynamics of the colicin Ia channel domain in the water-soluble and membrane-bound forms from dipolar couplings. (a) ^{13}C - ^1H DIPSHIFT time trace of Val C α in the water-soluble (dotted line, filled squares) and membrane-bound (solid line, open squares) states. (b) ^1H - ^1H dipolar coupling of the Ala C α cross section of the 2D WISE spectra. The membrane-bound protein (solid line) has smaller couplings than the water-soluble form (dotted line).

colicin Ia channel domain adopts an open and extended tertiary structure in the membrane, in contrast to the soluble state, which has a globular structure and which is nearly completely immobilized.⁵⁷ The dynamics of the membrane-bound colicin Ia channel domain is also influenced by the anionic lipid content of the membrane and the ionic strength of the buffer:⁵⁸ the protein is the most rigid under high-salt and low-anionic-lipid conditions, which correspond to the most physiological membrane surface potential. This suggests that optimum channel activity requires the colicin Ia channel domain to be sufficiently rigid to allow entire helices to undergo cooperative conformational changes, and these conformational changes are required for translocating the channel-forming helices across the lipid bilayer.

In membrane peptides such as M2TMP and TP-I, not only is there abundant side chain motion, but also there is large-amplitude backbone reorientation. Various spin interactions have been used to detect this backbone motion, including ²H quadrupolar coupling, C–H and N–H dipolar couplings, and ¹⁵N and ¹³CO chemical shift anisotropies.^{20,23,37} Since the backbone reorientation of small membrane peptides is usually uniaxial around the bilayer normal, the spectra exhibit $\eta = 0$ line shapes, and a magic-angle hole can be detected in the chemical shift spectra measured with ¹H cross-polarization. The magic-angle hole results from the collinearity of the motionally averaged X–H dipolar coupling tensor and the X-spin CSA tensor. At the isotropic shift, the X–H dipolar coupling vanishes, thus giving no CP signal. We found that PG-I undergoes fast uniaxial rotation in thin DLPC bilayers but becomes immobilized in thick POPC membranes.²⁰ In comparison, the β -hairpin peptide TP-I retains fast uniaxial mobility in thick POPC membranes. Moreover, TP-I is oriented parallel to the membrane surface; thus, its rotation affects a large area of lipid molecules, weakening the membrane structure. Comparative studies of several TP mutants suggest this uniaxial rotation to be essential for antimicrobial activity, as the lack of motion is correlated with low activity.

8. Summary

Solid-state NMR spectroscopy can be used to extract rich information on membrane protein structure and dynamics. We have reviewed here recently developed NMR techniques for determining the depth of insertion, orientation, and oligomeric structure of membrane proteins and highlighted their applications to several membrane peptides and proteins. Atomic- and nanometer-scale distances can now be measured with high precision. The solid-state NMR methods described here are best applied to membrane peptides and proteins whose basic secondary structure is more or less known, as is the case for the disulfide-stabilized β -hairpin antimicrobial peptides, but whose tertiary and quaternary structure are unknown. These techniques are thus complementary to multidimensional correlation experiments that permit the resonance assignment and site-resolved extraction of *intramolecular* distances and torsion angles (for a recent review, see ref 59). The development of these latter methods is a rapidly evolving field that is approaching solution NMR standards and has been demonstrated on increasingly large microcrystalline proteins. However, the three-dimensional structures of membrane proteins are incomplete without information about their insertion state, orientational angles, and oligomeric state in the lipid membrane. Therefore, a combination of the topological experiments described here and the resonance-assignment techniques will be important to fully elucidate the membrane-bound three-dimensional structure and dynamics and the lipid interaction of membrane proteins.

Acknowledgment. This work is contributed by a number of talented students and postdoctoral fellows, including Dr. S. Yamaguchi, Dr. J. Buffy, Dr. X. Yao, R. Mani, M. Tang, T. Doherty, S. Cady, and W. Luo. Financial support by the National Institutes of Health, National Science Foundation, and a Sloan Fellowship (to M.H.) is gratefully acknowledged.

References and Notes

- (1) Creighton, T. E. *Proteins: Structures and molecular properties*, 2nd ed.; W.H. Freeman and Co.: New York, 1993.
- (2) Zasloff, M. *Nature* **2002**, *415*, 389.
- (3) Fyfe, C. A. *Solid state NMR for chemists*; C. F. C. Press: Guelph, Ontario, 1983.
- (4) Schmidt-Rohr, K.; Spiess, H. W. *Multidimensional Solid-State NMR and Polymers*, 1st ed.; Academic Press: San Diego, CA, 1994.
- (5) Hong, M. *Acc. Chem. Res.* **2006**, *39*, 176.
- (6) Hong, M. *Structure* **2006**, *14*, 1731.
- (7) Huster, D. *Prog. Nucl. Magn. Reson. Spectrosc.* **2005**, *46*, 79.
- (8) Opella, S. J.; Marassi, F. M. *Chem. Rev.* **2004**, *104*, 3587.
- (9) Tycko, R. *Q. Rev. Biophys.* **2006**, *39*, 1.
- (10) Pouny, Y.; Rapaport, D.; Mor, A.; Nicolas, P.; Shai, Y. *Biochemistry* **1992**, *31*, 12416.
- (11) Ludtke, S. J.; He, K.; Heller, W. T.; Harroun, T. A.; Yang, L.; Huang, H. W. *Biochemistry* **1996**, *35*, 13723.
- (12) Matsuzaki, K.; Murase, O.; Fujii, N.; Miyajima, K. *Biochemistry* **1996**, *35*, 11361.
- (13) Henzler Wildman, K. A.; Lee, D. K.; Ramamoorthy, A. *Biochemistry* **2003**, *42*, 6545.
- (14) Buffy, J. J.; Hong, T.; Yamaguchi, S.; Waring, A.; Lehrer, R. I.; Hong, M. *Biophys. J.* **2003**, *85*, 2363.
- (15) Bloembergen, N. *J. Chem. Phys.* **1957**, *27*, 572.
- (16) Solomon, I. *Phys. Rev.* **1955**, *99*, 559.
- (17) White, S. H.; Wimley, W. C.; Selsted, M. E. *Curr. Opin. Struct. Biol.* **1995**, *5*, 521.
- (18) Wiener, M. C.; White, S. H. *Biophys. J.* **1992**, *61*, 434.
- (19) Huster, D.; Yao, X. L.; Hong, M. *J. Am. Chem. Soc.* **2002**, *124*, 874.
- (20) Buffy, J. J.; Waring, A. J.; Lehrer, R. I.; Hong, M. *Biochemistry* **2003**, *42*, 13725.
- (21) Mani, R.; Cady, S. D.; Tang, M.; Waring, A. J.; Lehrer, R. I.; Hong, M. *Proc. Natl. Acad. Sci. U.S.A.* **2006**, *103*, 16242.
- (22) Doherty, T.; Waring, A. J.; Hong, M. *Biochemistry* **2006**, *45*, 13323.
- (23) Hong, M.; Doherty, T. *Chem. Phys. Lett.* **2006**, *432*, 296.
- (24) Prosser, R. S.; Hwang, J. S.; Vold, R. R. *Biophys. J.* **1998**, *74*, 2405.
- (25) Prosser, R. S.; Bryant, H.; Bryant, R. G.; Vold, R. R. *J. Magn. Reson.* **1999**, *141*, 256.
- (26) De Angelis, A. A.; Jones, D. H.; Grant, C. V.; Park, S. H.; Mesleh, M. F.; Opella, S. J. *Methods Enzymol.* **2005**, *394*, 350.
- (27) Dvinskikh, S. V.; Dürr, U. H.; Yamamoto, K.; Ramamoorthy, A. *J. Am. Chem. Soc.* **2007**, *129*, 794.
- (28) Lu, J. X.; Damodaran, K.; Lorigan, G. A. *J. Magn. Reson.* **2006**, *178*, 283.
- (29) De Angelis, A. A.; Nevzorov, A. A.; Park, S. H.; Howell, S. C.; Mrse, A. A.; Opella, S. J. *J. Am. Chem. Soc.* **2004**, *126*, 15340.
- (30) Park, S. H.; Mrse, A. A.; Nevzorov, A. A.; De Angelis, A. A.; Opella, S. J. *J. Magn. Reson.* **2006**, *178*, 162.
- (31) Yamaguchi, S.; Waring, A.; Hong, T.; Lehrer, R.; Hong, M. *Biochemistry* **2002**, *41*, 9852.
- (32) Tang, M.; Waring, A. J.; Lehrer, R. I.; Hong, M. *Biophys. J.* **2006**, *90*, 3616.
- (33) Marassi, F. M.; Opella, S. J. *J. Magn. Reson.* **2000**, *144*, 150.
- (34) Wang, J.; Denny, J.; Tian, C.; Kim, S.; Mo, Y.; Kovacs, F.; Song, Z.; Nishimura, K.; Gan, Z.; Fu, R.; Quine, J. R.; Cross, T. A. *J. Magn. Reson.* **2000**, *144*, 162.
- (35) Saffman, P. G.; Delbruck, M. *Proc. Natl. Acad. Sci. U.S.A.* **1975**, *72*, 3111.
- (36) Aisenbrey, C.; Bechinger, B. *J. Am. Chem. Soc.* **2004**, *126*, 16676.
- (37) Cady, S. D.; Goodman, C.; Tatko, C. D.; DeGrado, W. F.; Hong, M. *J. Am. Chem. Soc.* **2007**, *129*, 5719.
- (38) Munowitz, M.; Aue, W. P.; Griffin, R. G. *J. Chem. Phys.* **1982**, *77*, 1686.
- (39) Nakamura, T.; Furunaka, H.; T, T. M.; Tokunaga, F.; Muta, T.; Iwanaga, S.; Niwa, M.; Takao, T.; Shimonishi, Y. *J. Biol. Chem.* **1988**, *263*, 16709.
- (40) Matsuzaki, K.; Nakayama, M.; Fukui, M.; Otaka, A.; Funakoshi, S.; Fujii, N.; Bessho, K.; Miyajima, K. *Biochemistry* **1993**, *32*, 11704.
- (41) deAzevedo, E. R.; Bonagamba, T. J.; Hu, W.; Schmidt-Rohr, K. *J. Am. Chem. Soc.* **1999**, *121*, 8411.

- (42) Buffy, J. J.; Waring, A. J.; Hong, M. *J. Am. Chem. Soc.* **2005**, *127*, 4477.
- (43) Luo, W.; Hong, M. *J. Am. Chem. Soc.* **2006**, *128*, 7242.
- (44) Bain, A. D. *Prog. Nucl. Magn. Reson. Spectrosc.* **2003**, *43*, 63.
- (45) Meier, B. H. *Adv. Magn. Opt. Reson.* **1994**, *18*, 1.
- (46) Vanderhart, D. L. *J. Magn. Reson.* **1987**, *72*, 13.
- (47) Schmidt-Rohr, K.; Hong, M. *J. Am. Chem. Soc.* **2003**, *125*, 5648.
- (48) Rienstra, C. M.; Tucker-Kellogg, L.; Jaroniec, C. P.; Hohwy, M.; Reif, B.; McMahon, M. T.; Tidor, B.; Lozano-Perez, T.; Griffin, R. G. *Proc. Natl. Acad. Sci. U.S.A.* **2002**, *99*, 10260.
- (49) Wi, S.; Sinha, N.; Hong, M. *J. Am. Chem. Soc.* **2004**, *126*, 12754.
- (50) Mani, R.; Tang, M.; Wu, X.; Buffy, J. J.; Waring, A. J.; Sherman, M. A.; Hong, M. *Biochemistry* **2006**, *45*, 8341.
- (51) Gullion, T.; Schaefer, J. *J. Magn. Reson.* **1989**, *81*, 196.
- (52) Tang, M.; Waring, A. J.; Hong, M. *J. Magn. Reson.* **2007**, *184*, 222.
- (53) Heller, H.; Schaefer, M.; Schulten, K. *J. Phys. Chem.* **1993**, *97*, 8343.
- (54) vanRossum, B. J.; deGroot, C. P.; Ladizhansky, V.; Vega, S.; deGroot, H. J. M. *J. Am. Chem. Soc.* **2000**, *122*, 3465.
- (55) Clauss, J.; Schmidt-Rohr, K.; Adam, A.; Boeffel, C.; Spiess, H. W. *Macromolecules* **1992**, *25*, 5208.
- (56) Huster, D.; Xiao, L. S.; Hong, M. *Biochemistry* **2001**, *40*, 7662.
- (57) Wiener, M.; Freymann, D.; Ghosh, P.; Stroud, R. M. *Nature* **1997**, *385*, 461.
- (58) Yao, X. L.; Hong, M. *Biochemistry* **2006**, *45*, 289.
- (59) McDermott, A. E. *Curr. Opin. Struct. Biol.* **2004**, *14*, 554.